

Experimental simulation of lightning optical emissions in clouds

Arindam Banerjee, Anil A Ogale and Kunal Mitra¹

Mechanical and Aerospace Engineering Department, Florida Institute of Technology, 150 W University Blvd, Melbourne, FL 32901, USA

E-mail: kmitra@fit.edu

Received 31 August 2005, in final form 29 November 2005

Published 20 January 2006

Online at stacks.iop.org/JPhysD/39/575

Abstract

The objective of the study is to experimentally determine the information content of lightning optical emissions through clouds. Clouds affect the amplitude of lightning signals and the apparent dimensions of the optical source. Multiple scattering from the cloud media also alters the shape of the temporal profile of the lightning signal. The goal is to provide accurate estimates of the arrival time delay and temporal pulse width broadening of output signals emitted from clouds for different cloud and lightning parameters. Experiments conducted in the laboratory yield a temporally broadened pulse with an overall decrease in the peak and a delay in the pulse rise time. Parameters such as optical thickness of the cloud medium and the scattering coefficients are varied to simulate different cloud properties. The experimental results are compared with a transient radiative transfer formulation solved using the discrete ordinate method. The practical implications of this research will be improved reliability on prediction of weather conditions, defence applications and geophysical applications like atmospheric studies.

1. Introduction

Lightning is a transient, high electric discharge phenomenon with path length of the order of a few kilometres. The National Aeronautics and Space Administration (NASA) classifies lightning into four groups: cloud-to-ground, cloud-to-cloud, cloud-to-air and inter-cloud lightning. Originating from the electric discharge in clouds [1, 2], lightning has a very non-linear mode of propagation. Lightning is an indicator of convection and precipitation and thus is an indicator of the total rain volume in clouds. Clouds affect both atmospheric hydrological and energy cycles. Since precipitation is a basic component of the hydrological cycle [3, 4], it thus becomes very important to estimate the moisture content of clouds. Latent heat released from clouds affects sea surface salinity, ocean circulation and ultimately the overall climate [5]. Clouds are assumed to be composed of a homogeneous collection of identical spherical water droplets, each droplet being a nearly conservative anisotropic scatterer with a highly forward elongated phase function. Clouds affect the amplitude of

lightning signals and the apparent dimensions of the optical source. Multiple scattering from the cloud media also alters the shape of the temporal profile of the lightning signal. The presence of such media will delay the arrival of several photons due to multiple scattering. This would imply an overall decrease in the observed peak, a delay in pulse rise time and an overall pulse broadening effect. Details of the cloud properties can be observed in various features of back scattered light as well as forward scattered light [6]. This necessitates the development of reliable monitoring methods and at the same time the development of accurate numerical models to study the information content in a lightning system.

Lightning detection over the years has predominantly been divided into different categories based on the available technology of the detectors. They include radio frequency (RF) detectors, interferometers, optical monitors and atmospheric field mill monitors [7]. Apart from these, there are a variety of hybrid designs which use a combination of the other single-technology designs. Atmospheric measurements are often flawed by poor knowledge and control on the governing parameters. Multilayered clouds, changes in cloud water droplet size and phase (ice or water) are some parameters which

¹ Author to whom correspondence should be addressed.

contribute to erroneous results in remote sensing systems [8,9]. This has led to the use of satellites for lightning detection [10]. Satellite observations of lightning have been gathered over the years and details of a comprehensive space-based lightning detection system have been addressed [10, 11]. Remote detection of lightning has also been characterized to compare the pulse characteristics of intra-cloud and cloud-to-cloud lightning using the lightning mapper system [12]. Detection of lightning signals will provide accurate estimate of cloud properties and, in turn, the atmospheric conditions. Such information is crucial in applications ranging from aviation safety to defence and commercial applications like geophysical and atmospheric studies. The method of using Bernoulli's form of the propagation equation (a partial differential equation combining scattering and extinction properties of the atmosphere) has been proposed as early as 1954 to retrieve the signal reflectivity and attenuations in rain from radar returns [13]. A stable analytical inversion for LIDAR (Light Detection and Ranging) returns was first proposed by Klett [14]. This solution is then applied to invert LIDAR returns.

Several numerical models have been proposed for a more accurate prediction of the cloud properties. Models to predict the electromagnetic fields associated with lightning have been developed extensively [15]. A diffusion model for lightning produced photons in optically thick thunderclouds using a one speed Boltzmann transport theory has been proposed [6]. The concept of inverse modelling of the transport equation to predict the properties of cloud have been studied [16]. A numerical model for laser transmissions through cirrus cloud has been developed [17]. Various models have been proposed for the understanding of the lightning return stroke. Rakov and Uman suggested four models for modelling of the lightning strokes [18]. Unfortunately, most of these methods deal with steady state-reflection, transmission and absorption of radiation in a semi-infinite plane parallel to clouds. The steady-state assumption is inadequate in the case of lightning and models must include the transient term when accounting for the propagation of lightning. There has been a lack of research on the development and experimental validation of the transient numerical models available for analysing the data from space borne measurement systems.

The study of actual lightning in open atmosphere and modelling of the results obtained is very expensive and difficult to achieve. Also it has its limitations because of the restrictions due to instrumentations used and uncertainty in weather conditions. This places a severe restriction on the pace of development of new technology. To overcome these shortcomings, laboratory simulation of lightning gains much significance. This would also allow us a greater control on the involved parameters allowing more detailed studies. Experiments conducted in laboratory are more cost effective than in field testing during the initial stages where fundamental issues need to be resolved. Laboratory scale experiments on lightning involve simulating lightning by generating an electrical streamer in a gaseous medium by inducing a breakdown. This is achieved by passing high energy short pulse laser through the medium. For example, plasma breakdown by passing high energy electrons has been studied for beam propagation over long distances [19].

Since the early 1980s, there has been rapid progress in ultra-fast laser technology. The development of chirped-pulse amplifications and titanium-doped sapphire (Ti:sapphire) as the lasing medium has made available pulsed laser systems with pulse duration in the order of nanoseconds to femtoseconds [20]. Laser profiling is the simplest application of the LIDAR technique. In this method a short pulse of light (visible or near infrared) is emitted and the reflected signal detected after a finite time. By measuring the time delay and knowing the speed of propagation of the pulse, the range from the instrument can be determined. Similarly if a continuous stream of pulses is used a profile of the range can be built.

The objective of this work is to determine the information content of the lightning optical emissions through clouds by laboratory simulation of lightning using a short pulse laser as a lightning source. The advantage of this is that the distortion in the temporal profile of the output pulse which is of the same order of the lightning channel can be observed. Lightning behaviour over path lengths can be controlled by varying the optical depth of the cloud medium. Ideally, experiments should be performed using water vapour as a cloud medium instead of fog. However, it is extremely difficult to maintain the vapour state as water vapour condenses with time and this alters the optical properties during the experiment. Thus a commercial fog generator is used to create a fog-cloud medium for the experiment. Experimental measurements are compared with numerical simulation results obtained by solving the transient radiative transfer equation (RTE) using the discrete ordinates method (DOM) [21]. The effects of medium properties such as fog-cloud medium thickness, number density of the fog-cloud particles on the scattered temporal transmitted and reflected signals are examined. Scattered optical signals are also measured at various angles from the incident light axis. Numerical simulation of lightning parameters such as variation of the temporal width of the lightning channel is also performed to analyse the effect on the temporal scattered signals.

2. Experimental set-up

A mode-locked argon ion short pulse laser source having a pulse width of 230 ps and repetition rate of 76 MHz is used as a lighting source for experimental purpose. The incident pulse width is continuously monitored during the experiment using an ultra fast photo-detector (New-focus, Model 1954) coupled to an oscilloscope (Tektronix 7S11, 7T11). The optical path length is controlled using a pair of dielectric mirrors (New Focus 5151 VIS) mounted on translation stages. Attenuators are used to control the incident power. The stray light as well as the reflected light is minimized using a mask on both sides of the chamber. The detection is done using a Hamamatsu streak camera (C-1587) coupled with a CCD camera (Model # C-4742-95). The streak camera is equipped with an ultra fast synchroscan unit (M1955) coupled with the frequency tuning unit (M1954). The streak camera has a temporal resolution of 10 ps. The setup is remotely controlled using the HPDTA-32 data acquisition software [22]. The details of the setup are illustrated in figure 1(a). The streak camera is triggered at the mode locking frequency of the laser.

Clouds are simulated using fog entrapped in a chamber. The fog-cloud chamber is made of plexiglass and the walls are

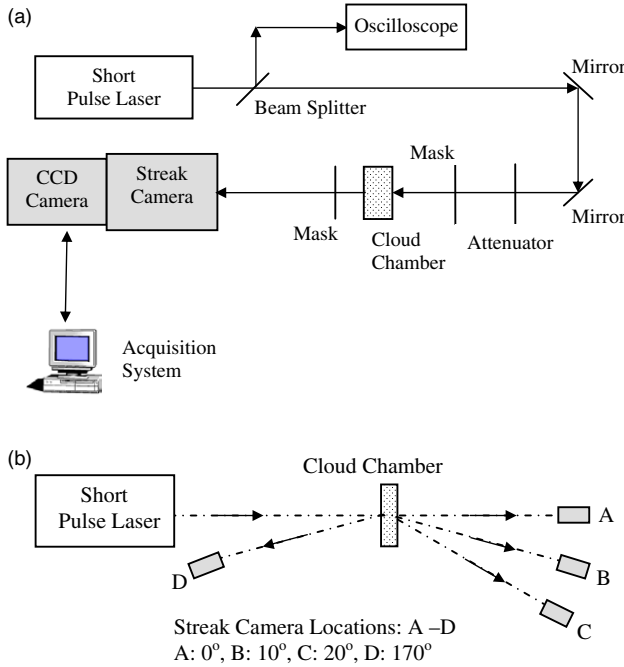


Figure 1. (a) Schematic of the experimental set-up. (b) Location of the streak camera for angular measurements.

(This figure is in colour only in the electronic version)

sealed with silicone. The depth of the chamber (D) is varied from 25.4 to 76.2 mm to simulate different optical depths. A ball valve is attached at the top to control the amount of fog–cloud to be filled in. The fog–cloud is generated using a fog machine (Maxi Fogger). Experiments are performed immediately after the chamber is filled with fog–cloud to avoid condensation and formation of fog–cloud droplets on the chamber walls. The cloud chamber is placed in the path of the laser beam with the incident surface at right angles to the beam. A mask is used on both sides of the cloud chamber to reduce surrounding stray light and maximize the efficiency of the streak camera. The streak camera is positioned at various positions around the cloud chamber to facilitate measurement of the scattered optical signal at various angular locations as shown in figure 1(b).

The scattering coefficient of the cloud medium is varied by controlling the amount of fog–cloud inside the chamber. The fog–cloud properties are approximated from the Mie scattering theory [23]. A mean fog–cloud particle diameter ($2a$) of $0.5 \mu\text{m}$ and a refractive index of the fog–cloud medium of 1.5 as provided by the manufacturers is used for estimating the optical properties. For an incident wavelength of 532 nm, a size factor (x_s) of 2.953 is obtained. It was assumed that the sphere was large such that it is sufficient to resort to geometric optics when evaluating the scattering efficiency. Thus as a first approximation, Q_{ext} is assumed to have a value of 2 [23]. Furthermore as it is considered a highly scattering medium the scattering efficiency factor (Q_{sca}) is taken to be 1.9, which gives an absorption efficiency factor (Q_{abs}) of 0.1. The volume of each particle (V_p) is found to be $6.54 \times 10^{-14} \text{ cm}^3$. Since the specific gravity of fog–cloud is 1.044 (as taken from the data sheet provided by the manufacturer), the mass of each fog–cloud particle (m_p) is found to be $6.83 \times 10^{-14} \text{ g}$. The

total mass of the fog–cloud filled inside the chamber (M_t) is noted before each run. For a chamber filled with 400 g of fog, the number of particles ($N_p = M_t/m_p$) is calculated as 5.85×10^9 particles. The number density ($N_d = N_p/V_{\text{chamber}}$) of the particles for this case is $2.23 \times 10^4 \text{ cm}^{-3}$. The values of the scattering coefficient ($\sigma_s = \pi a^2 Q_{\text{sca}} N_d$) and the absorption coefficient ($\sigma_a = \pi a^2 Q_{\text{abs}} N_d$) [23] are found to be 0.8 and 0.044 mm^{-1} . The optical depth is given as a product of the medium thickness (D) and the extinction coefficient ($\sigma_e = \sigma_s + \sigma_a$). The optical depth is varied by varying either the medium thickness or the scattering coefficient. Three different scattering coefficients of the cloud medium of 0.8, 1.6 and 2.4 mm^{-1} as well as three different medium thicknesses of 25.4, 50.8 and 76.2 mm are used for the experiments.

3. Theory

In this study the medium is approximated by an anisotropic scattering and absorbing rectangular enclosure. The RTE in a given direction Ω is given by

$$\frac{1}{c} \frac{\partial I(x, y, \Omega, t)}{\partial t} + \mu \frac{\partial I(x, y, \Omega, t)}{\partial x} + \eta \frac{\partial I(x, y, \Omega, t)}{\partial y} + \sigma_e I(x, y, \Omega, t) = \frac{\sigma_s}{4\pi} \int_{4\pi} \Phi(\Omega', \Omega) I(x, y, \Omega', t) d\Omega' + S(x, y, \Omega, t), \quad (1)$$

where, I is the scattered diffuse intensity ($\text{Wm}^{-2} \text{ sr}^{-1}$), σ_e and σ_s are the extinction coefficient and the scattering coefficient, respectively, Φ is the phase function, Ω is the direction cosine, c is the velocity of light in the medium, x and y are the spatial coordinates, t is the time and S is the source term [12, 23]. To account for the Gaussian nature of the incident laser pulse ideally a cylindrical coordinate system with an axis-symmetric geometry should be used. But because the cloud chamber is rectangular in shape, a two-dimensional Cartesian coordinate system is used with finer grids near the incident laser face to account for the Gaussian nature of the incident laser pulse. As soon as the laser pulse enters the cloud chamber it suffers random scattering and so the use of two-dimensional Cartesian coordinate geometry is sufficient. A similar model has been used to analyse short pulse laser propagation through tissue medium and good agreement between modelling results and experimental measurements has been obtained [24]. The scattering phase function can be represented in a series of Legendre polynomials P_k by

$$\Phi(\Omega', \Omega) = \sum_{k=0}^K a_k P_k[\cos(\Theta)], \quad (2a)$$

where a_k are the associated coefficients in the expansion. A value of $K = 1$ and $a_k = -1, 0$ and 1 corresponds to a linear backward, isotropic and a linear forward phase function, respectively. The higher the value of K the more forward or backward scattered is the phase function depending on the value of a_k . In this paper a value of $K = 1$ and $a_k = 1$ is used. The scattering angle Θ is represented by

$$\cos(\Theta) = \mu\mu' + \eta\eta' + \xi\xi', \quad (2b)$$

where μ , η and ξ are the direction cosines of the light propagation direction Ω , and μ' , η' and ξ' are the direction

cosines corresponding to the angle of scatter with respect to the same co-ordinate system. The pulsed radiation incident on the medium is a square-shaped pulse with a temporal duration (pulse width), t_p at full width half-maximum (FWHM). The intensity can be separated into a collimated component, corresponding to the incident source, and a scattered intensity. If I_c is the collimated intensity, then I is the remaining intensity described by equation (1). The collimated component of the intensity for the square pulse is represented by

$$I_c(x, y, \Omega, t) = I_0 e^{-\sigma_e x} [H(t - x/c) - H(t - t_p - x/c)] \delta(\Omega - \Omega_0), \quad (3)$$

where I_0 is the intensity leaving the wall towards the medium, $H(t)$ the Heaviside step function, and $\delta(t)$ the Dirac delta function. The source function S formed from the collimated irradiation is then given by

$$S(x, y, \Omega, t) = \frac{\sigma_s}{4\pi} \int_{4\pi} \Phi(\Omega', \Omega) I_c(x, y, \Omega', t) d\Omega'. \quad (4)$$

For a collimated pulsed laser radiation, the associated boundary condition at this surface can be written as

$$I_0(\Omega, t) = \varepsilon q_0 \delta(\Omega - \Omega_0) + \frac{1 - \varepsilon}{\pi} \int_{n_s \cdot \Omega' > 0} n_s \cdot \Omega' I^{in} d\Omega', \quad (5)$$

$$n_s \cdot \Omega < 0,$$

where ε is the emissivity of the wall, q_0 is the radiative flux in the direction of the collimated incident radiation, n_s is the unit outward normal vector at the boundary and I^{in} is the intensity coming from the medium towards the laser incident surface. In equation (5) the first and the second terms represent emitted and reflected components of the boundary intensity, respectively. The reflected term is composed of the irradiation due to diffuse and collimated radiation. To study primarily the effect of a square short-pulse collimated radiation, the emission and reflection from the medium and its boundaries are neglected except for the laser incident face.

3.1. Discrete ordinates method

The DOM is based on a discrete representation of the directional variation of the radiative intensity. The RTE and the associated boundary condition are replaced with a set of equations for a finite number of M directions that cover 4π sr solid angles [25]. As such, the DOM is simply a finite differencing of the directional dependence of the equation of transfer. Integrals over solid angles are approximated by numerical quadrature. The DOM requires a single formulation to invoke higher order approximation, integrates easily into control volume transport code and is applicable to Mie anisotropic scattering phase function and inhomogeneous media. Discrete ordinates have also been widely used for solution of the transient radiative transport equation [21, 26].

The integral terms of equations (1) and (4) are reformulated with the aid of an angular quadrature of order M . The discrete form of the time-dependent radiative transport equation in the direction Ω_m is then represented as

$$\frac{1}{c} \frac{\partial I_m(x, y, t)}{\partial t} + \mu_m \frac{\partial I_m(x, y, t)}{\partial x} + \eta_m \frac{\partial I_m(x, y, t)}{\partial y} = -\sigma_e I_m(x, y, t) + \frac{\sigma_s}{4\pi} \sum_{m'=1}^M w_{m'} \Phi_{m'm} I_{m'}(x, y, t) + S_m(x, y, t), \quad (6)$$

where $m = -M, \dots, -1, 1, \dots, M$, $\{\Omega_m, w_m\}$ defines a quadrature of M discrete directions Ω_m with which the weights w_m are associated. Details of the solution procedure, as previously developed are not repeated here and can be found in the literature [21].

4. Results

The objective of this study is to analyse the information content of lightning emissions through clouds. This necessitates that the lightning channel output pulsed signal be plotted as a function of time. A streak camera is used to detect the temporal variation in the pulse profile. The temporal variation in the pulse profile contains information about the cloud properties. The experimental results along with the corresponding numerical results are presented in this section. Numerical results are obtained by solving equation (6). The streak camera is placed at various orientations with respect to the incident beam.

Normalized scattered transmitted and reflected signals are plotted as a function of time. As the intensity obtained from the streak camera is not calibrated, the intensity values are normalized with respect to the maximum intensity values for the corresponding observations. This allows for comparison between experimental measurements and numerical modelling results. Figure 2 shows the comparison between experimental and numerical results for varying fog–cloud medium thickness for a detection angle of 180° (transmission). For an incident pulse width of 230 ps, temporally broadened pulses having FWHM equal to 287 ps, 403 ps and 480 ps are obtained experimentally for a fog–cloud medium thickness of 25.4 mm, 50.8 mm and 76.2 mm, respectively. The broadened pulse FWHM for the numerical runs are 293 ps, 411 ps and 486 ps for the three thicknesses, respectively. Thus, it is observed that the experimental and numerical results are in conformity with each other and are within the resolution error of the camera. The increase in broadening of the pulse width with an increase in fog–cloud medium thickness can be explained by the fact that when light passes through a highly scattering medium such as clouds it is subjected to multiple scattering because of numerous collisions with the particles of the medium. Almost all the photons experience a number of collisions before exiting through the medium and arrive later than the original pulse. These photons carry information about the optical properties of the fog–cloud medium. Thus the greater the medium thickness the higher the temporal broadening with a longer decaying tail.

It can be observed that even if the optical depth of the medium is kept constant by varying the values of the scattering coefficient and medium thickness, the broadening of the scattered pulse (FWHM) is not the same (table 1). This would suggest that FWHM of the temporally broadened pulse should be considered independent functions of the scattering coefficient and the medium thickness and not a combined effect of the optical depth. An increase in the medium thickness is found to have more impact on pulse broadening than an increase in the scattering coefficient. The difference in the time of the earliest arriving photon of the scattered pulse in figure 2 is because of the time of flight of photons inside the medium. This delay (t_d) can be found out as ($t_d = D \times n/c_v$), where n is the

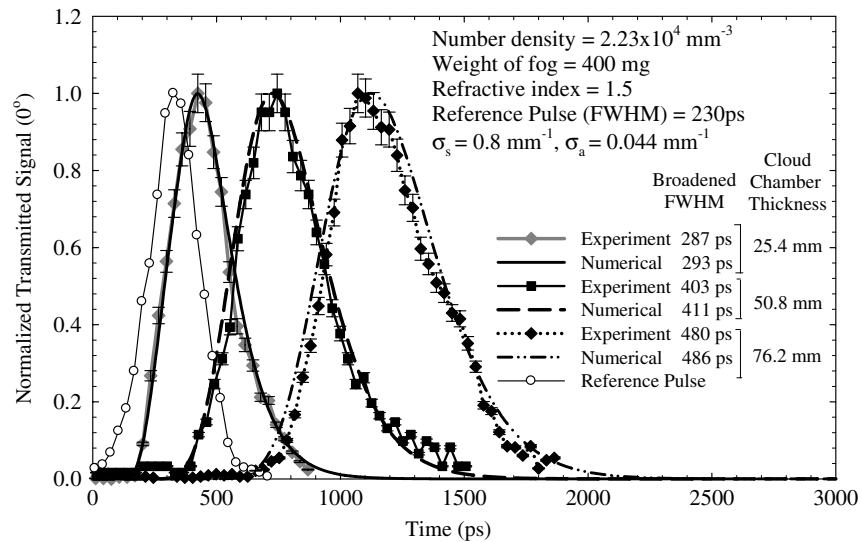


Figure 2. Effect of medium thickness on the forward transmitted signal along the optical axis.

Table 1. Comparison of FWHM for different optical depths.

Medium thickness (D) mm	Extinction coefficient (σ_e) mm^{-1}	Optical depth ($D \times \sigma_e$)	Temporally broadened pulse width FWHM (ps)
25.4	0.84	21.36	293
25.4	1.64	41.64	343
50.8	0.84		403
25.4	2.64	61.96	393
76.2	0.84		480

refractive index of the medium, D is the medium thickness and c_v is the speed of light in vacuum. For example, the time needed for the earliest arriving photon to traverse a 25.4 mm thick fog–cloud medium having a refractive index of 1.5 is 56.44 ps. It is evident from figure 2 that as the medium thickness increases the delay time before any appreciable scattered signal also increases. As the intensity values are normalized for the purpose of comparison the actual intensity levels are masked. The intensity of the scattered light decreases with an increase in the scattering coefficient as well as an increase in the medium thickness. Similar trends are observed at detection angles of 10° and 20° with respect to the optical axis and are not presented here.

Uncertainty in experimental observations is an important parameter which has to be accounted for when analysing the scattered optical signals. The laser pulse width is a function of the laser power and varies with a change in the laser power. Although the laser power fluctuates within a range of 10 mW, the pulse width can be assumed to be constant during the duration of the experiment. The time resolution obtained by the streak camera with the experimental setup used is about 10 ps for a reference pulse of 230 ps (5%). If variations in consecutive readings obtained are more than 5% then they are neglected. The spatial resolution of the camera depends upon the settings made during the focusing operation. As these settings are not changed for the entire experiment the spatial resolution of the camera remains the same. Uncertainty analysis is performed for the fog–cloud medium thicknesses of 25.4, 50.8 and 76.2 mm and having $\sigma_s = 0.8 \text{ mm}^{-1}$,

$\sigma_a = 0.044 \text{ mm}^{-1}$ as shown in figure 2. The repeatability of measured optical signals is within 2.5% as is evident from the uncertainty bars.

Figure 3 shows the effect of different scattering coefficients ($\sigma_s = 0.8, 1.6$ and 2.4 mm^{-1}) on scattered transmitted signal detected at an angle of 0° to the incident light axis for a 25.4 mm thick fog–cloud medium. It can be observed that as the scattering coefficient of the medium is increased, the temporal broadening of the pulse (FWHM) increases considerably.

The effect of the detection angle on scattered signal is shown in figure 4. As the detection angle is varied from 0° (transmitted beam) to 170° (reflected beam), a large variation in the intensity of the scattered signal is observed. The maximum intensity values are obtained for back scattered signals whereas maximum broadening is observed for the forward scattering signal along the optical axis (0°). It is observed that as the forward detection angle is changed from 0° to 20° a decrease in the pulse broadening is seen. In figure 4 intensity values are not normalized to illustrate the difference in the intensity levels of the scattered signal.

Figures 5 and 6 show the effect of the variation of scattering coefficient and medium thickness on the back scattered signal measured at a detection angle of 170° to the optical light axis. Measurements are not made at an angle of 180° since detection of the direct reflected signal (180°) is not possible due to interference with the incident laser beam. However, it is of interest to know how the direct reflected signal (180°) would behave for each of these cases and hence numerical simulations of reflected signals are performed at an angle of 180° . Figure 5 shows a comparison of the experimental results (at a 170° detection angle) with the numerical results for a reflected signal (at a 180° detection angle). It is seen that the rise times are fairly uniform between the experimental and numerical data for all the three cases. However, since the numerically obtained output signals are measured at an angle of 180° , the temporal width of the signals is considerably wider than the experimentally obtained signals

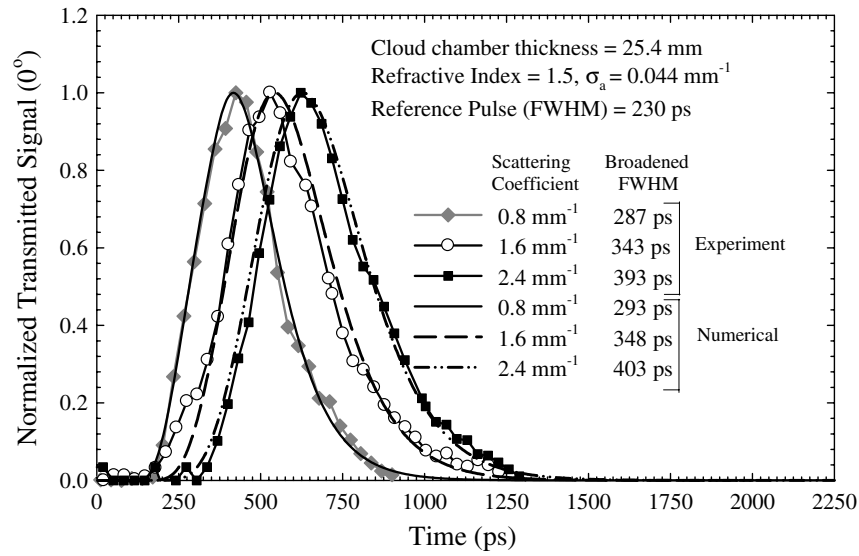


Figure 3. Effect of scattering coefficient of fog–cloud particles on forward transmitted signal along the optical axis.

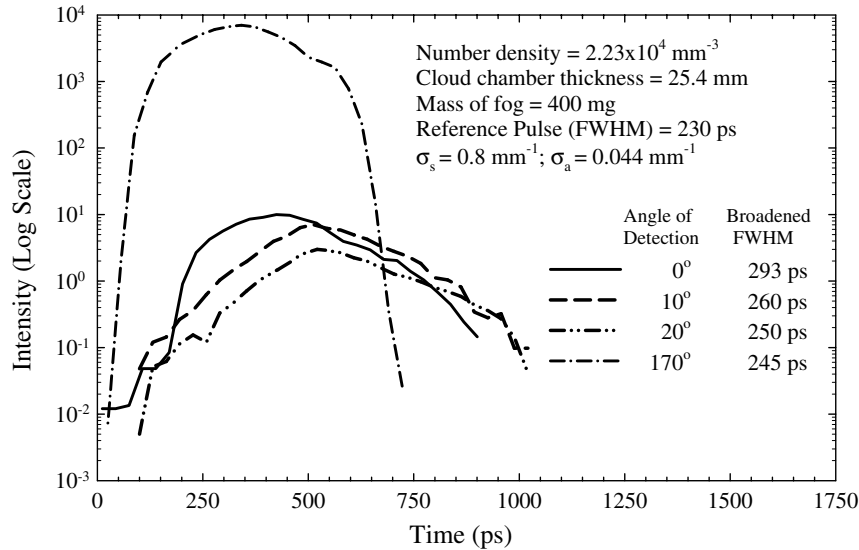


Figure 4. Effect of angular variation of the scattered signal.

measured at 170°. A similar trend is observed for the case when the chamber thickness is varied as in figure 6.

Temporal width of the lightning signal is varied numerically to illustrate the importance of the transient effect for analysis of the lightning optical emission through fog–cloud media. Figure 7 shows the temporal profiles of scattered transmitted signal obtained numerically for various temporal widths of the lightning channel. The numerical simulation is performed for a fog–cloud chamber of thickness 25.4 mm with $\sigma_s = 0.8 \text{ mm}^{-1}$ and $\sigma_a = 0.044 \text{ mm}^{-1}$. The importance of the transient effect for the analysis of the lightning signal is clearly demonstrated when the temporal width of the lightning signal is considerably smaller than the characteristic propagation time in the fog–cloud medium, which for a 25.4 mm thick fog–cloud medium having a refractive index of 1.5 is 56.44 ps. It is noted that for such cases, the temporal broadening of the transmitted signal (FWHM) is considerably larger than the temporal width of the lightning signal. In the case of the lightning signal

having a temporal width of $t_p = 2 \text{ ps}$ (which is roughly 1/30th of the propagation time), the transmitted signal has a fast response at early time instants and then a long decaying tail. The temporally broadened output pulse width (FWHM) of the scattered beam is 177 ps. With the increase of the lightning signal temporal width to $t_p = 20 \text{ ps}$, the temporal broadening of transmitted pulse (FWHM) changes to around 180 ps. In the case of an incident temporal pulse width of 230 ps (as used for the experiments), the incident width is around 4 times larger than the propagation time of the lightning in the medium. The temporal broadening of the transmitted pulse is observed to be around 293 ps numerically. Thus information about fog–cloud media characteristics depends on the temporal width of the lightning channels.

Determination of fog–cloud medium characteristics requires inverse modelling of the transient RTE, which is complicated to solve. For comparison between numerical and experimental results plotted in figure 2, the values of scattering

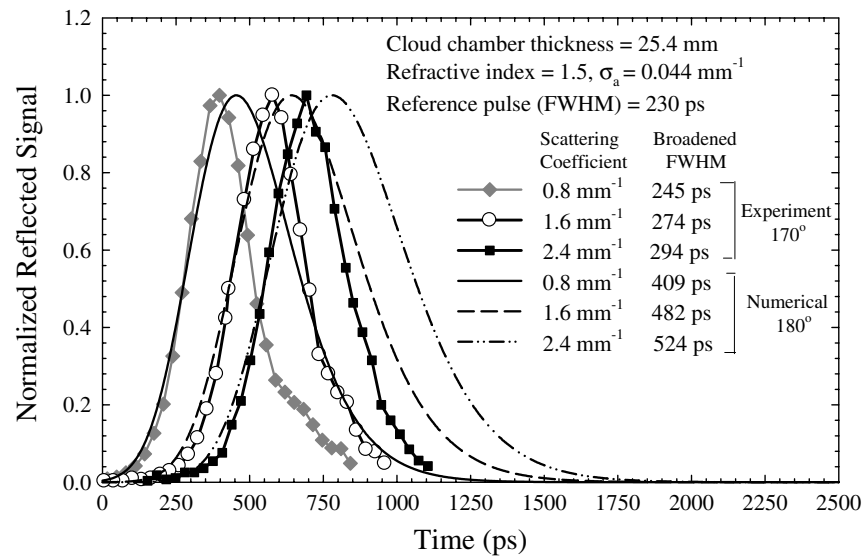


Figure 5. Effect of scattering coefficient on the back scattered signal.

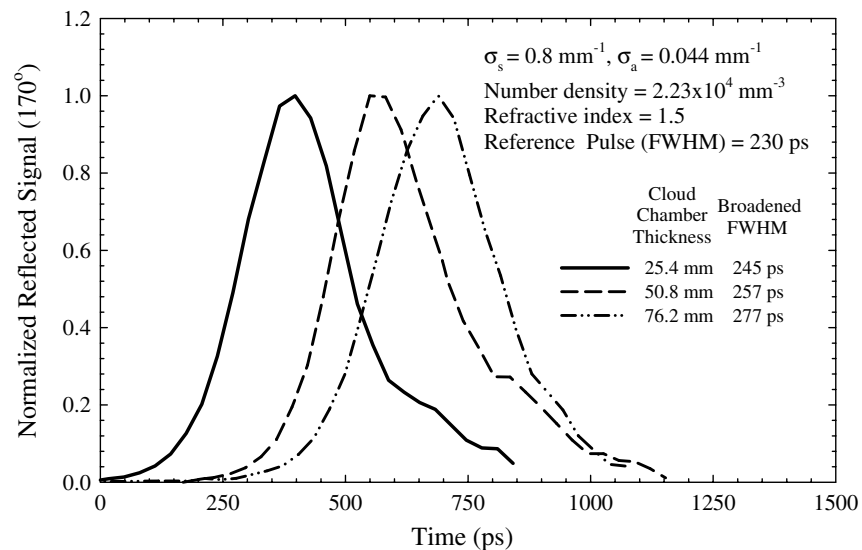


Figure 6. Effect of fog–cloud medium thickness on back scattered signal measured at an angle of 170°.

and absorption coefficients are estimated from the amount of fog–cloud filled in the chamber. These values are used in the numerical computations. For the case shown below in figure 8 the numerical profile is generated iteratively using different values of scattering and absorption coefficient until a match with the experimental results is obtained. The scattering and absorption coefficients that match are then used to back calculate the mass of the fog. Numerical back calculation yielded a 1006 mg of fog–cloud used for an actual value of 1000 mg of fog–cloud used and it can be concluded that the method used is accurate.

5. Conclusion

This research is one of the first studies undertaken to simulate lightning studies on a laboratory scale using short pulsed laser as a lightning source. Cloud medium is simulated using a fog–cloud filled in a chamber. Experimental results obtained

are compared with a transient numerical radiative transport equation solved using a DOM. It is observed that when a lightning channel passes through a highly scattering medium such as clouds, an increase in the output pulse width or the phenomenon of temporal pulse broadening is observed. An increase in the pulse width is observed with an increase in the optical depth of the medium. This is attributed to multiple scatterings taking place inside the medium. The experimental results obtained are within 2% of the numerically predicted results which is well within the permissible error range of 5% in the pulse width. This shows the validity of the measurement approach used. Depending upon the angle of detection, different magnitudes of intensities and temporal pulse broadening are observed. The present results also suggest that temporal pulse broadening should be considered an individually dependent function of the scattering coefficient and the medium thickness rather than a collective function of the optical depth. The effect of medium thickness is found to

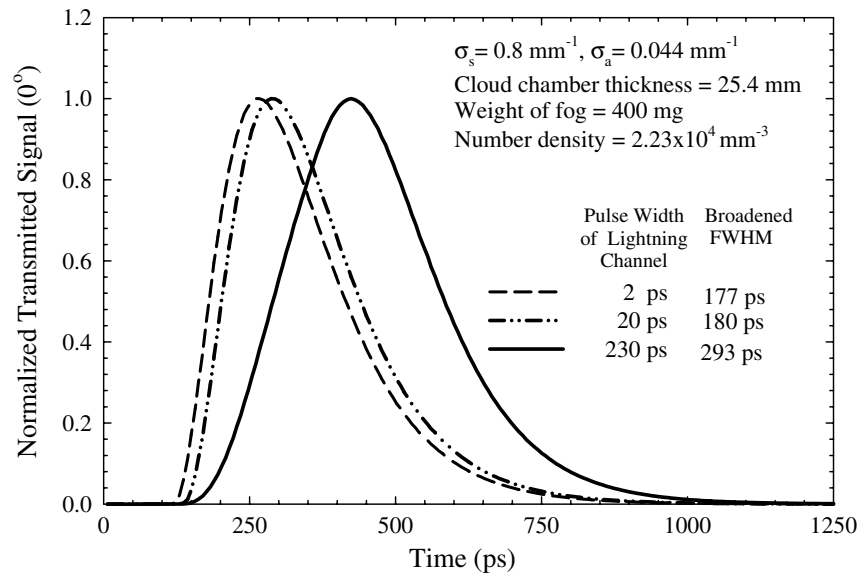


Figure 7. Effect of pulse width of lightning channel on forward transmitted signal along the optical axis.

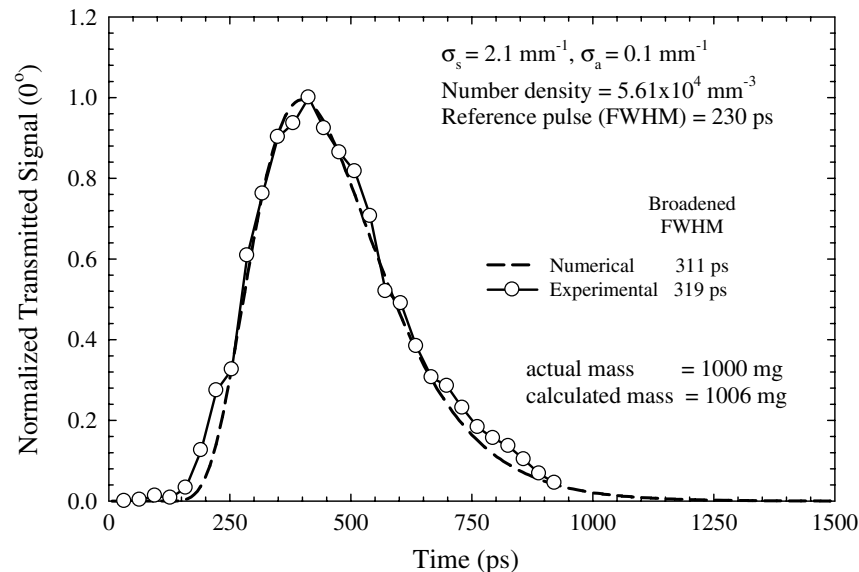


Figure 8. An inverse approach of numerical matching on experimental data to obtain the mass of the fog–cloud.

have a greater impact on the forward scattering signal. This study can be further expanded using water vapour as a cloud medium instead of fog.

Acknowledgments

The authors wish to acknowledge the Florida Space Grant Consortium for providing the financial support for the project.

References

[1] Lupò G, Petrarca C, Tucci V and Vitelli 2000 *IEEE Trans. Electromagn. Compat.* **EMC-42** 39–53
 [2] Uman M A 1982 A review of natural lightning: experimental data and modeling *IEEE Trans. Electromagn. Compat.* **EMC-24** 79–112

[3] Goodman S J and MacGorman D R 1986 Cloud-to-ground lightning activity in mesoscale convective complexes *Mon. Weather Rev.* **114** 2320–2328
 [4] Goodman S J and Buechler D E 1990 Lightning rainfall relationships *Proc. American Meteorological Society Conf. on Operational Precipitation Estimation and Prediction (Anaheim, CA, February 1990)*
 [5] Bing L, Patric M, Bruce W, David R D, Rabindra P, David F Y and Taneil U 1998 Estimation of water cloud properties from satellite microwave, infrared and visible measurements in oceanic environments 2: results *J. Geophys. Res.* **103** 3887–905
 [6] Koshak W J, Solakiewicz R J, Phanord D D and Blakeslee R J 1994 Diffusion model for lightning radiative transfer *J. Geophys. Res.* **99** 14361–71
 [7] Hasbrouck R T 1990 Lightning. Understanding it and protecting systems from its effects *Instrum. Aerospace Ind. Proc. ISA Aerospace Instr. Sym.* **36** 601–38

- [8] Wielicki B A, Cess R D, King D, Randall A and Harrison E F 1995 Mission to planet earth: role of clouds and radiation in climate *Bull. Am. Meteor. Soc.* **76** 2125–53
- [9] Gupta S K, Darnell W L and Wilber A C 1992 A parameterization for surface longwave radiation from satellite data: recent improvements *J. Appl. Meteor.* **31** 1361–7
- [10] Christian H J, Blakeslee R J and Goodman S J 1989 The detection of lightning from geostationary orbit *J. Geophys. Res.* **93** 13329–37
- [11] Orville R E and Henderson R 1986 Global distribution of midnight lightning: September 1977 to August 1978 *Mon. Weather Rev.* **114** 2640–53
- [12] Goodman S J, Christian H J and Rust W D 1988 A comparison of the optical pulse characteristics of intracloud and cloud-to-ground lightning as observed above cloud's *J. Appl. Meteor.* **27** 1369–81
- [13] Hitschfeld W and Bordan J 1954 Errors inherent in the radar measurement of rainfall at attenuating wavelengths *J. Appl. Meteor.* **11** 58–64
- [14] Klett J D 1981 Stable analytical inversion solution for processing lidar returns *Appl. Opt.* **20** 211–20
- [15] Lupò G, Petrarca C, Tucci V and Vitelli M 2000 EM fields associated with lightning channels: on the effect of tortuosity and branching *IEEE Trans. Electromagn. Compat.* **42** 394–404
- [16] Czerwiński M, Mrockza J, Girasole T, Gouesbet G and Gréhan G 2001 Light transmittance predictions under multiple-light-scattering conditions: I. Direct problem: hybrid-method approximation *Appl. Opt.* **40** 1514–24
- [17] Liou KN, Takano Y, Ou S C and Johnson M W 2000 Laser transmission through thin cirrus clouds *Appl. Opt.* **39** 4886–94
- [18] Rakov V A and Uman M A 1998 Review and evaluation of lightning return stroke models including some aspects of their application *IEEE Trans. Electromagn. Compat.* **40** 403–1426
- [19] Barov N, Conde M E, Gai W and Rosenzweig J B 1998 Propagation of short electron pulses in a plasma channel *Phys. Rev. Lett.* **80** 81–4
- [20] Strickland D and Mourou G 1985 Compression of amplified chirped optical pulses *Opt. Commun.* **56** 219–21
- [21] Sakami M, Mitra K and Hsu P 2002 Analysis of light-pulse transport through two-dimensional scattering-absorbing media *J. Quant. Spectrosc. Radiat. Transfer* **73** 169–79
- [22] Ogale A A 2002 Study of lightning through clouds using short pulse lasers *Thesis Mechanical and Aerospace Engineering, Florida Institute of Technology*
- [23] Modest M F 1993 *Radiative Heat Transfer* (New York: McGraw Hill)
- [24] Trivedi A, Basu S and Mitra K 2005 Temporal Analysis of Reflected Optical Signals for Short Pulse Laser Interaction with Nonhomogeneous Tissue Phantoms *J. Quant. Spectrosc. Radiat. Transfer* **93** 337–48
- [25] Fiveland W A 1988 Three dimensional radiative heat transfer solution by the discrete ordinates method *J. Thermophys. Heat Transfer* **2** 309–16
- [26] Sakami M, Mitra K and Vo-Dinh T 2002 Analysis of short-pulse laser photon transport through tissues for optical tomography *Opt. Lett.* **27** 336–8